Effect of graphene oxide on the hydration process and macro-mechanical properties of cement

Lounis Djenaoucine[a], Alvaro Picazo[b], Miguel Angel de la Rubia[a], Jaime Carlos Gálvez[a],*, Amparo Moragues[a]

[a] *Department of Civil Engineering: Construction, School of Civil Engineering, Technical University of Madrid, C/ Profesor Aranguren s/n, 28040 Madrid, Spain*
[b] *Department of Building Technology, Superior Technical School of Building, Technical University of Madrid, Avda. Juan de Herrera 6, 28040 Madrid, Spain*

ARTICLE INFO

ABSTRACT

The impact of graphene oxide (GO) on the hydration process, calcium silicate hydrate (C—S—H) gels structure, and macro-mechanical properties were systematically researched by combinatorial techniques. Findings from ^{29}Si MAS-NMR and nitrogen adsorption (BET) revealed that the effect of GO on the hydration degree of the cement paste, and the main chain length (MCL) is more pronounced at advanced ages (from 28 days), due to its act as a nucleation site. Moreover, the results of Raman spectroscopy tests showed that GO has a strong interaction with the cement matrix. Due to the increase in the degree of hydration, the lengthening of the chain length (MCL), and the formation of strong bonds, both compressive and flexural strength tests also improved. Therefore, the effect of GO as a nucleation site has a positive effect on the cement paste nano-properties at advanced ages.

Efecto del óxido de grafeno en el proceso de hidratación y las propiedades macromecánicas del cemento

RESUMEN

Palabras clave:
Óxido de grafeno
Cemento
Longitud de cadena media
Grado de hidratación
Propiedades de resistencia

El impacto del óxido de grafeno (GO) en el proceso de hidratación, la estructura de los geles de silicato de calcio (C—S—H) y las propiedades macromecánicas, se investigó sistemáticamente mediante técnicas combinadas. Los resultados de la resonancia magnética (RM) de silicio de ^{29}Si y la adsorción de nitrógeno (BET) revelaron que el efecto del GO en el grado de hidratación y la longitud de cadena media (MCL) de la pasta de cemento es más pronunciado a edades avanzadas (desde los 28 días) debido a su función como sitio de nucleación. Además, los resultados de los ensayos de espectroscopía Raman mostraron que el GO tiene

* *Corresponding author.*
E-mail address: jaime.galvez@upm.es (J.C. Gálvez).

una fuerte interacción con la matriz de cemento. Debido al aumento del grado de hidratación, el alargamiento de la MCL y la formación de enlaces fuertes, también mejoraron tanto la resistencia a la compresión como las de flexión. Por lo tanto, el efecto del GO como sitio de nucleación tiene un efecto positivo en las nano propiedades de la pasta de cemento en edades avanzadas.

Introduction

Nanotechnology is a growing area of science and engineering that seeks to understand and manipulate matter at the nanometer scale [1]. Consequently, it is regarded as one of the most promising research areas in several sectors, including building materials. In recent years, the advanced state of nanotechnology has paved the way for nanomaterials as the most reliable way to enhance cement composite performance such as strength and durability [2]. Overall, two significant mechanisms have been highlighted for improving the cement composite performance through the incorporation of nanomaterials. First, nanomaterials with a high specific surface area may serve as hydration products nucleation sites, resulting in an acceleration of the hydration process and the generation of more hydration products such as (C—S—H) gel, therefore achieving the desired results [3,4], since the (C—S—H) gel is the main component that contributes significantly to the cohesion and strength of cement composite [5]. Second, nanomaterials can plug and seal the pores in cement, making it more compact [6,7].

Several research findings have shown that including nanomaterials can achieve better strength and durability of cement composites to varying degrees. For example, nano-silica (n-SiO$_2$) can enhance the hydration degree, especially early due to its nucleation effect and the pozzolanic reaction [8,9]. Nano-alumina (n-Al$_2$O$_3$) may provide more surface area for precipitation and the development of hydration products due to its high specific surface area [10]. Carbon nanotubes (CNTs) may lower the porosity of Portland cement since it can function as a filler between hydration products [11,12].

The graphene oxide (GO) nanomaterial has attracted the interest of many researchers as a viable nano-strengthening agent in cement composites [4,6,13,14]. GO contains oxygenated functional groups, such as hydroxyls and epoxides at the basal plane and carbonyls and carboxylates at the edge. These functional groups facilitate its dispersion in aqueous solutions. This remarkable property, coupled with its outstanding mechanical properties, renders GO a promising and versatile nanomaterial for enhancing the performance of cementitious composites [15].

Most studies are focused on the mechanical strength and durability of GO-modified cement such as concrete mortar and paste. Mokhtar et al. [7] showed that when 0.02% GO nanoplatelets were added to cement paste, the compressive strength grew by 13% while the indirect tensile strength rose by about 41% when 0.03% was added, compared with the reference sample. Gong et al. [16] showed that the admixture of GO nanosheets at 0.03% in cement paste increases the compressive and tensile strength by more than 40% and decreases the overall porosity of the cement paste. According to Pan et al. [13] cement composites compressive and flexural strengths are increased by 33% and 58%, respectively, when 0.05% GO is added.

In this context, more rigorous research at the nanoscale is needed to research the function of GO in the hydration process of cement composites and to establish the source of macro-level enhancements or constraints. According to the above-cited study of Pan et al. [13], the mechanical strength of GO-modified cement composite can be enhanced owing to the ability to react carboxylic acid groups with (C—S—H) gel to generate strong covalent bonds and may also increase of (C—S—H) gel specific surface area. The study by Lin et al. [4] has shown the significant role of GO in stimulating the cement hydration process, as the oxygen-containing functional groups of GO serve as adsorption sites for both water and cement components as well as seeding sites for cement hydration products. Furthermore, nuclear magnetic resonance ^{29}Si MAS-NMR studies on tricalcium silicate (C$_3$S) conducted by Kang and Yang [17,18] showed that adding GO in different proportions increased the hydration degree but no change was noticed in GO-modified cement paste structure.

However, according to contradicting research, GO had no substantial influence on the hydration of cement. As stated by Wang et al. [19] GO does not enhance the process of hydration but affects the hydration product morphology and crystallization. Horszczaruk et al. [20] also showed that the incorporation of GO into the cement has no strong effect on the hydration process. Additionally, the GO-modified sample had a nearly similar morphology to the reference material, which means that the crystal phases were retained when GO was incorporated.

This research aims to elucidate the role of GO in the performance of cementitious materials. The influence of GO-modified cement paste on the hydration kinetics and the chain structure of calcium silicate hydrate (C—S—H) was investigated by means of ^{29}Si MAS-NMR characterization method. Additionally, Raman spectroscopy was employed to explore the possible interactions between GO and the hydration products of cement. Moreover, the impact of GO on the specific surface area of C—S—H gel was assessed by nitrogen adsorption technique. Based on the results acquired at the nanoscale, the metrics for boosting the mechanical properties of GO-modified cement mortar are also detailed in this study.
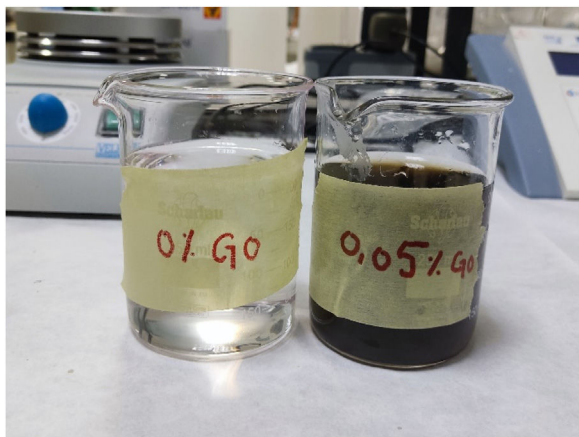
Table 1 – Chemical composition of Portland cement used by XRF (wt.%).										
Wt.%	Al_2O_3	SiO_2	CaO	Fe_2O_3	K_2O	MgO	Na_2O	TiO_2	P_2O_5	SO_3	LoI
CEM I	5.03	20.5	61.5	3.20	1.05	1.45	0.15	0.25	0.19	3.35	2.39

Note. LoI: loss on ignition; XRF: X-ray fluorescence.

Table 2 – Chemical composition of GO (www.graphenea.com).				
Carbon	Hydrogen	Nitrogen	Sulphur	Oxygen
49–56	0–1	0–1	0–2	41–50

Fig. 1 – GO-water suspension prepared.

Materials and methods

Materials

The cement used in this study was ordinary Portland cement I 52.5R, and its chemical composition is shown in Table 1. A GO commercial solution with a concentration of 4 g/l was used. Table 2 shows the chemical composition of GO. Furthermore, CEN-NOMRSAND standardized sand was used for mortar, according to the EN 196-1 standard [21], arranged in bags with 1350 ± 5 g content.

Preparation of GO-water suspension

This study utilized a GO solution with a concentration of 0.05% (by mass of cement). A control batch without GO (0% GO) was also prepared for comparative purposes. The two dosages were denoted as BDGO_0 and BDGO_05, respectively, indicating 'Basic Dilution of Graphene Oxide' (Fig. 1 shows the prepared solutions). The volume of the GO solution corresponding to the weight of the dose was pipetted into a pipette and then poured into the distilled water. Next, the solution was stirred with a magnetic stirrer for 5 min at a rotational speed of 800 rpm. It is important to mention that in the preparation of the cement paste and mortar, graphene oxide (GO) was added to the mixture without reducing the total weight of the cement. The weight of the GO used is so small that it does not significantly affect the overall mass of the cement. Therefore, adding GO supplements the cement rather than replacing any part of it.

Preparation of GO-cement paste

Once the dose of GO-water was prepared, the dose was placed in an automatic rotary mixer containing the required cement (Table 3 lists the mix proportions of the GO-modified cement paste, with a constant 0.5 w/c ratio). The kneading process starts at a low speed and lasts 90 s. After a 30-s pause, the paste was mixed again at low speed for 90 s. After the mixing process was completed, the cement paste was poured into molds in the form of a prismatic bar (10 mm × 10 mm × 60 mm) in two layers, each layer being compacted with 60 strokes. Lastly, the mold was covered with a plastic sheet and placed in a curing chamber with controlled ambient conditions ($20 \pm 2\,°C$/RH > 95%). All samples were de-molded after 24 h and kept in the curing chamber at the same conditions until the test day.

Preparation of GO-cement mortar

To test the mechanical properties (compressive and flexural strength), cement mortar named MBDGO_0 and MBDGO_05 were prepared following the European standard EN 196-1:2018 [21]. The prepared GO-water solution was placed in the mixing bowl along with the required cement (Table 3 lists the mix proportions of the GO-modified cement mortar with a constant 0.5 w/c ratio). The process of mixing began at a slow rate for 30 s, followed by a consistent addition of sand for a further 30 s, then a 90-s pause, after which the mixing process recommenced at a rapid pace for 60 s. After completion of the mixing process, the fresh mixture was poured into prismatic molds (160 mm × 40 mm × 40 mm) in the form of two layers, each layer was compacted with 60 strokes, then the mixture was covered with plastic sheet and the molds were kept in the curing chamber under ambient conditions ($20 \pm 2\,°C$/RH > 95%). All samples were de-molded after 24 h and stored in the curing chamber for different times until testing.

Characterization techniques

^{29}Si magic angle spinning nuclear magnetic resonance ^{29}Si MAS-NMR

^{29}Si MAS-NMR was performed on crushed cement paste samples (BDGO_0 and BDGO_05) at 7, 28 and 90 days using a Bruker Spectrometer model AV400 MHz WB with a resonant frequency of 79.5 MHz, spinning speed of 10 kHz and 4 μs for pulse width. Chemical shifts of ^{29}Si were referenced to tetramethylsilane (TMS) at 0 parts per million (ppm). The

Table 3 – Mix proportions of cement paste and mortar.								
Mix proportion	Cement (g)	Sand (g)	w/c	Water content (ml)			GO (%)	GO (mg)
				Distilled water	GO dispersion 4 g/l	Total water		
Cement paste								
BDGO_0	450	–	0.5	225	0	225	0	0
BDGO_05	450	–	0.5	168.75	56.25	225	0.05	225
Cement mortar								
MBDGO_0	450	1350	0.5	225	0	225	0	0
MBDGO_05	450	1350	0.5	168.75	56.25	225	0.05	225

data were processed using the commercial NMR software MestRenova, and the curve generated was constrained by the Gauss–Lorentz function.

BET

Nitrogen adsorption test was performed on crushed cement paste samples powder (BDGO_0 and BDGO_05) at 28 days to determine the specific surface area as well as the pore size distribution. The samples were degassed for 2 h at 90 °C before analysis to remove water and organic vapor, roughly 0.5 g of powder was measured from each cement paste sample. The specific surface areas of cement samples were evaluated using the Brunauer–Emmet–Teller (BET). The BET study relies on the amount of N_2 (nitrogen) gas adsorbed at different partial pressures (from 0.01 to 0.30 P/P_0).

Raman spectroscopy

Confocal Raman spectroscopy was used to assess whether GO and cement gel (C—S—H) form an interaction at 28 days of curing. The experimental Raman spectra were obtained using a Witec Micro-Raman Confocal coupled with an AFM (ALPHA 300RA), with a Nd:YAG laser excitation at 532 nm (green laser) and an oil immersion 100 objective (NA = 0.9). The laser power used for the measurements was as low as 0.7 mW to minimize as much as possible the heating effect over the powders due to the high absorption of GO powders. The optical resolution of the confocal microscope was limited to 200 nm in the lateral direction and to 500 nm in the vertical direction.

Raman spectral resolution of the system is down to 0.02 cm^{-1}. The microscope base was also equipped with an active vibration isolation system, active in the range of 0.7–1000 Hz. The acquired spectrum was processed and analyzed using the WITec Project 2.02 program, which allows a specific, sensitive, immune to interferences and non-intrusive analysis of crystals and provides a method for characterizing chemical properties of heterogeneous samples, with great resolution and rapid data. The duration for spectrum collection was 10 s and the laser spot size was 50 μm. The spectra were scanned across a range of 100 cm^{-1} to 3700 cm^{-1}.

Macro-mechanical strength

Flexural and compressive strength testing of GO-modified cement mortar samples (MBDGO_0 and MBDGO_05) was carried out using a three-point bending machine (Ibertest C1B1400) and a hydraulic machine (Ibertest model HIB 150), respectively, with 40 mm × 40 mm × 160 mm prismatic specimens at 2, 7, 28 and 90 days, following the procedures specified in the standard EN 196-1: 2018 [21]. The average flexural
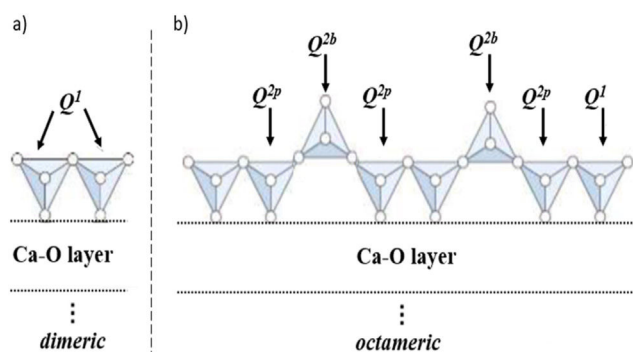

Fig. 2 – Schematic diagram of silicate chain. (a) Dimeric and (b) octameric.
Adapted from Ref. [26].

strength was obtained after conducting a test of three samples for each type and the remaining two halves of each sample of flexural test were used to test the compressive strength and calculate the average.

Results and discussion

^{29}Si MAS-NMR analysis

The hydration degree and (C—S—H) gel structure of crushed cement pastes (BDGO_0 and BDGO_05) were determined using ^{29}Si MAS-NMR spectroscopy after 7, 28, and 90 days of curing to obtain a deeper insight into (C—S—H) gel, which is the main hydration product contributing to the cohesion and strength of cementitious materials [5]. Furthermore, this allows for the observation of GO-induced changes in the (C—S—H) gel structure. According to Taylor's research [5], the (C—S—H) gel is a poorly crystalline product with a tobermorite-like structure, which is composed of a layer of CaO and two silicate tetrahedral chains, where the structural alterations in (C—S—H) gel is mainly caused by the change in the peak intensity and chemical shifts.

According to the findings of prior studies. Q^n species silicate structures ($n = 0$–4), where Q denotes the silicate tetrahedron and n denotes the number of oxygen atoms interacting with nearby tetrahedrons, according to Fig. 2. The shift around −68 to −74 ppm is associated with Q^0 which represents the tetrahedral silica of unreacted C_2S and C_3S in the cement paste. The shift located between −76 to −80 ppm is Q^1, representing the end of silicate tetrahedra. As well Q^2 at −81.5 to −85.5 ppm

(a) BDGO_0 at 7 days

(b) BDGO_05 at 7 days

(c) BDGO_0 at 28 days

(d) BDGO_05 at 28 days

(e) BDGO_0 at 90 days
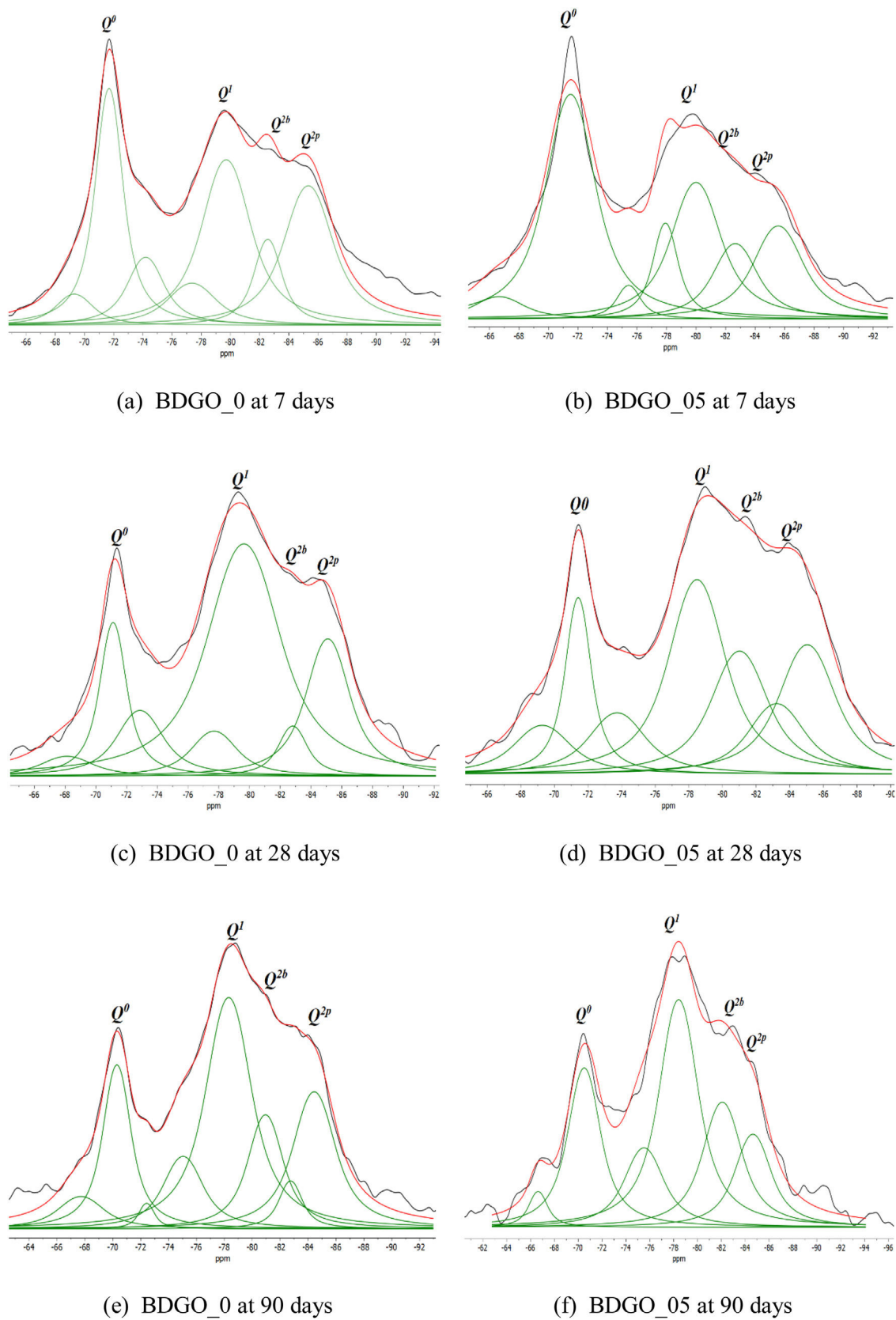
(f) BDGO_05 at 90 days

Fig. 3 – Deconvoluted ^{29}Si MAS-NMR spectra of BDGO_0 and BDGO_05 at 7, 28, and 90 days: (a, c, e) BDGO_0; (b, d, f) BDGO_05.

Table 4 – Deconvolution results of ^{29}Si MAS-NMR spectra at 7, 28, and 90 days.						
Sample	Q^0 (%)	Q^1 (%)	Q^{2b} (%)	Q^{2p} (%)	α (%)	MCL
7 days						
BDGO_0	43.53	34.05	8.97	13.45	56.47	3.32
BDGO_05	44.94	34.65	9.20	11.21	55.06	3.18
28 days						
BDGO_0	28.56	46.81	9.59	15.04	71.44	3.05
BDGO_05	26.70	44.76	12.06	16.48	73.30	3.28
90 days						
BDGO_0	26.33	47.42	10.68	15.57	73.67	3.11
BDGO_05	23.81	44.75	13.71	17.73	76.19	3.41

approximately, represents the center site of the silicate chain, Q^2 may be further split into the bridging and pairing sites Q^{2b} and Q^{2p} respectively [22]. In this study, comparable results to previous studies were obtained [17,18,23]. As shown in Fig. 3, all absorption peaks for both samples (BDGO_0 and BDGO_05) are situated at the same position which means that in both samples there are identical elements of the (C—S—H) gel components. Furthermore, the changing peak intensities highlight the variation in the chain structure, from the tabulated data obtained from the curves, using the integral peaks intensities Q^n. The mean chain length (MCL), and the hydration degree (α) of (C—S—H) gel were estimated based Eqs. (1) and (2), respectively [24,25].

$$MCL = \frac{2 \times (Q^1 + Q^{2b} + Q^{2p})}{Q^1} \quad (1)$$

$$\alpha = \frac{Q^1 + Q^{2b} + Q^{2p}}{Q^0 + Q^1 + Q^{2b} + Q^{2p}} \times 100 \quad (2)$$

From the results shown in Table 4, it can be seen that at 7 days the hydration degree (α) together with the main chain length (MCL) of BDGO_0 was higher than BDGO_05. The reason may be related to the large specific surface area and hydrophilic nature of GO. At the beginning of mixing, GO absorbs a certain quantity of water, resulting in a deficiency of water required by the cement for the reaction.

These researchers [27–29] revealed in their studies that the interlayer spacing of GO influences water absorption in several ways. They demonstrated that inserting oxygen functional groups into GO increases the interlayer spacing distances, which may enhance its absorption capacity. Therefore, since cement paste containing GO had less water, certain cement particles did not fully react and remained unhydrated. Consequently, the hydration process is slowed. The research conducted by Li et al. [30] yielded comparable findings. They affirmed that GO inhibits a certain way in the hydration process at early age due to its absorption of water, which leads to a decrease in the cement hydration degree.

At 28 and 90 days, the hydration degree and main chain length (MCL) of BDGO_05 improved compared with BDGO_0. The hydration degree of BDGO_05 raised by 2.54% and 3.31% at 28 and 90 days, respectively, compared with BDGO_0. Furthermore, BDGO_05 exhibited greater main chain lengths of 7.01% and 8.80% at 28 and 90 days, respectively, compared with BDGO_0.

More detailed: first, the improvement in the hydration degree of BDGO_05 at an advanced age, can be attributed to the gradual release of water held between GO sheets over time. Moreover, the released water reacts with the cement components, to form more hydration products such as (C—S—H) gel, on top of the GO surface. Therefore, an increase in the degree of hydration was observed compared to the reference sample. It is also feasible, that the (C—S—H) gel formation may occur in GO interlayers, whereby, as mentioned previously, an amount of water can be stored between the GO layers. Therefore, a hydration process can occur inside GO, and a formation of (C—S—H) gel on top of the GO layers. This is known as the effect of GO as a nucleation site. These improvements stem not only from GO's nucleation effect but also from its ability to serve as the internal curing effect of GO after long-term hydration. Due to its large surface area and hydrophilic oxygen functional groups, GO acts as a water reservoir within the cement paste, preventing free water from evaporating too quickly. As the hydration process continues, and free water becomes less available, GO gradually releases its stored water to ensure continuous hydration [31,32]. This hypothesis can be corroborated, by a considerable drop in the Q^0 peak intensity with increases in the intensity if Q^1, Q^{2b} and Q^{2p} peaks, in the BDGO_05 sample compared with the BDGO_0 sample at 28 and 90 days. Therefore, indicates that more alite (C$_3$S) and belite (C$_2$S) were consumed and hydrated to produce more (C—S—H) gel. As a result, the produced (C—S—H) gel, is deposited on the GO layers, due to the higher surface energy of GO. Consequently, GO might be considered to serve as a nucleation site.

Secondly, as can be seen from Table 4 and Fig. 3, the BDGO_05 sample had a higher percentage of tetrahedral SiO$_4$ occupying Q^{2b} than the reference sample BDGO_0 at 28 and 90 days. This implies that the cement particles, which underwent hydration over time, generated more tetrahedral SiO$_4$ occupying Q^{2b} sites (bridge). Consequently, these SiO$_4$, which are formed over time, contributed to chain elongation of C—S—H, by transforming dimers into n-union monomers (e.g., trimers, pentamers, octamers), due to its act as a connection point between two short main chains (Fig. 2(a) and (b)).

Similar results were found by Zhao et al. [23], who reported that the effect of GO sheet as a nucleation site causes an increase in the main chain length of (C—S—H) gel. Finally, it can be concluded that the nucleation site effect of GO enhanced slightly the hydration process and increased the main chain length at an advanced age.
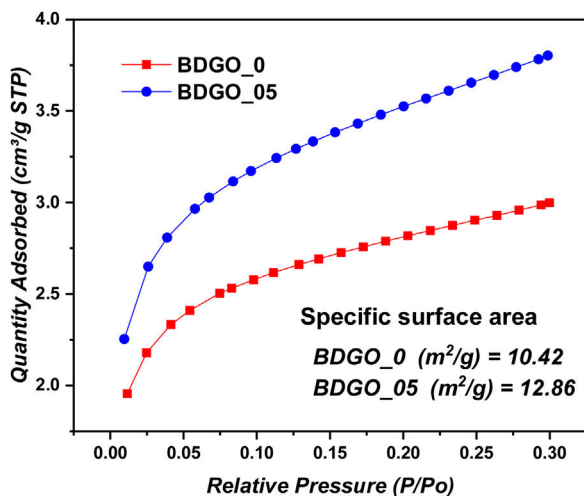
Fig. 4 – BET analysis of nitrogen adsorption isotherm and specific surface area of BDGO_0 and BDGO_05 at 28 days.

Fig. 5 – Raman spectra of pure GO and BDGO_05 at 28 days.

BET specific surface area

Another significant parameter related to the hydration degree was addressed in this study, which is the specific surface area of (C—S—H) gel. Nitrogen gas adsorption is a common way to figure out the cement specific surface area and pore structure. As mentioned in most studies, the specific surface area measured by the nitrogen adsorption technique (BET) in cement paste comes from (C—S—H) gel, where the specific surface area growth in the cementitious system is closely related to the development of the highly porous phase [13,23,33–35]. Fig. 4 shows the specific surface area and pore size distribution of samples BDGO_0 and BDGO_05 at the age of 28 days. Regarding the adsorption process, in Fig. 4 can be seen at all applied relative pressures, from $P/P_0 = 0.01$–0.3. Sample BDGO_05 adsorbed a greater amount of nitrogen compared with sample BDGO_0. The difference in the amount of nitrogen adsorbed between the two samples increases with increasing relative pressure. At the applied final relative pressure, $P/P_0 = 0.3$, the amount of nitrogen adsorbed from the BDGO_05 sample was 26.82% greater than the amount adsorbed from the BDGO_0 sample. This result shows that GO can expand the pore volume of the (C—S—H) gel. As we can see from prior ^{29}Si MAS-NMR results, at 28 days, GO enhances hydration process, implying the creation of more (C—S—H) gel, and it is plausible that increasing the (C—S—H) gel amount increases the gel pore proportions and their volume.

The specific surface area of the C—S—H gel of cement is a measure of how much surface area is available for adsorption of gas molecules. Regarding specific surface area, the incorporation of GO into the cement paste increased the specific surface area of (C—S—H) gel from $10.42\,\text{m}^2/\text{g}$ to $12.86\,\text{m}^2/\text{g}$, it is estimated that the rate of increase is 18.97%. Therefore, a logical interpretation of the results is that the increase in surface area indicates that the addition of GO promotes hydration over time. Also, it is plausible that the addition of nanomaterial such as GO with a high specific surface area can significantly increase the specific surface area of the sample and especially could serve for the increasing number of seeding sites. These
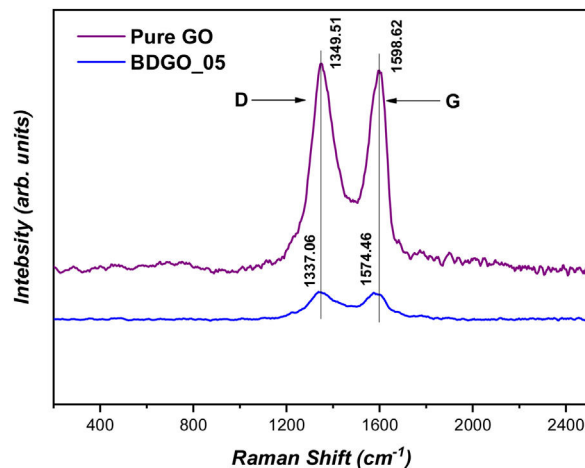
results are consistent with the previously reported results of ^{29}Si MAS-NMR and are also in agreement with previous studies [13,23,36]. Furthermore, the BET surface area rises with the addition of GO, indicating that the presence of GO promotes a seeding effect, hence increasing the MCL of the C—S—H gel as seen in NMR results.

Raman

As previously stated, GO can serve as a platform for (C—S—H) gel deposition. Therefore, this provides the potential for the formation of bonds between (C—S—H) gel and GO. In order to ascertain whether there is any interaction between (C—S—H) gel and GO, Raman spectroscopy was employed due to its high sensitivity to the electronic structure C=C [37].

Fig. 5 illustrates the Raman spectra of pure GO and GO embedded in the cement matrix. Raman spectra ranged in frequency from $200\,\text{cm}^{-1}$ to $2500\,\text{cm}^{-1}$. According to previous research [38,39] overall, Raman spectra of GO display two prominent Raman peaks at $\sim 1349\,\text{cm}^{-1}$ and $1598\,\text{cm}^{-1}$, where $1349\,\text{cm}^{-1}$ corresponds to the disordered state of carbon (D) specifically associated with a certain fraction of sp^3-bonded (tetrahedral) carbons, and the second one, $1598\,\text{cm}^{-1}$, corresponds to the graphitic carbon (ordered state, G), sp^2-bonded (trigonal) carbons.

As depicted in Fig. 5 a considerable shift of the Raman bands (D) and (G) were observed. Moreover, compared with the Raman spectrum of pure GO, the Raman shift of the D-band of GO introduced in the cement matrix shifted from $1337.06\,\text{cm}^{-1}$ to $1349.51\,\text{cm}^{-1}$, while the second peak corresponding to the G-band shifted from $1574.46\,\text{cm}^{-1}$ to $1598.62\,\text{cm}^{-1}$, which means quite a bit of wavenumber shift with the order of $12.45\,\text{cm}^{-1}$ for the D-band and $24.16\,\text{cm}^{-1}$ for the D-band. This behavior would indicate an increase of the bonding force constant, that is, the covalent C—C bond in the graphitic plane decreases in strength consequence of a strong interaction with the cement matrix. Therefore both, crystalline and amorphous structures of GO could be supporting compression by the cementitious matrix, also giving place to a broadening of the Raman modes D and G indicating a decrease in the force constant of both order and disorder states or bonds.
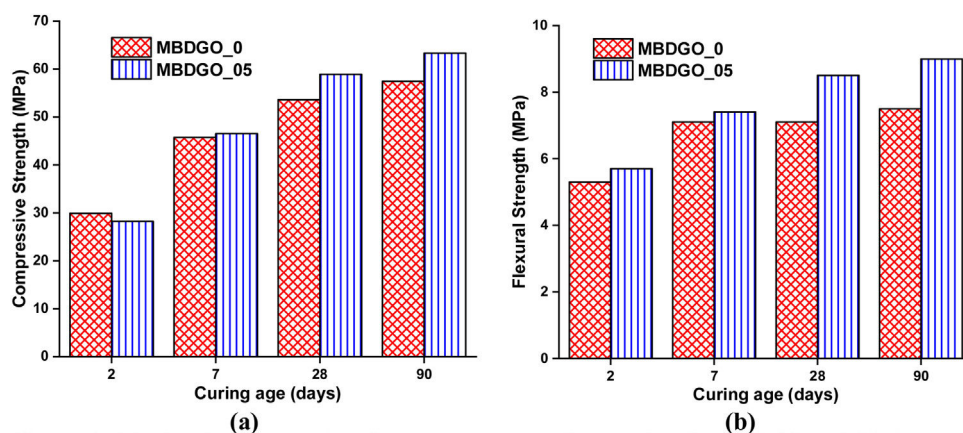
Fig. 6 – **Mechanical strengths of cement mortar after curing for 2, 7, 28 and 90 days: (a) compressive and (b) flexural.**

Similar results were found in the Yushi's et al. study [40], where they reported that there is a shift in both bands D and G estimated by 10 cm^{-1}, for CNF embedded in cement matrix compared to pure CNF (knowing that both GO, and CNF are carbon-based materials). Consequently, it was argued that the shift observed provides persuasive and unmistakable proof of the presence of interaction between CNF and cement matrix.

Besides, the ratio intensity of the D and G bands (I_D/I_G) is performed to determine the defect density of GO embedded in the cement matrix compared with pure GO. In our study, it was found that the I_D/I_G ratio of GO embedded in a cement matrix is 1.08 while the I_D/I_G ratio of pure GO is 0.96. That is an estimated difference of approximately 12.38%. Whereas the difference in the intensity of the two ratios, confirms the change in the carbon structure, i.e., the presence of intrinsic defects such as point defects caused by induced vacuum atoms in GO when mixed into the cement matrix [38,41]. GO's intrinsic defects may serve as active sites in chemical interactions, which have a significant impact on cement hydration. Finally, based on the Raman results, it can be confirmed that there is a strong interaction between GO and the cement matrix due to the attachment of hydration products on the surface of GO. In turn, this supports the above results of ^{29}Si-NMR and BET, that GO can act as a nucleation site for hydration products. As a consequence, an improvement in the degree of hydration was achieved.

Macro-mechanical strength

The effects of GO on the compressive and flexural strength of mortars were studied at 2, 7, 28, and 90 days, and the results are depicted in Fig. 6. At 2 and 7 days, the addition of GO did not improve the compressive strength of the mortar. In addition, in the flexural strength test, some improvements were observed in MBDGO_05, but they are still slight, compared with the reference sample MBDGO_0.

After 28 and 90 days, the compressive strength of sample MBDGO_05 increased by 9.33% and 10.45%, respectively, compared to the reference sample MBDGO_0. In terms of flexural strength, the sample MBDGO_05 outperformed the reference sample MBDGO_0 by 19.72% and 21.6% after 28 and 90 days, respectively.

In the first days, until 7 days as can be seen in ^{29}Si MAS-NMR results, GO did not affect the hydration process of cement paste. In GO-modified cement paste BDGO_05, the hydration degree and main chain length (MCL) were lower compared to the reference sample BDGO_0. As a conclusion, we found that GO did not affect the mortar's strength such as compressive and flexural, on 2 and 7 days.

Nevertheless, the findings were achieved at an advanced age, 28 and 90 days. As stated, above in ^{29}Si MAS-NMR, and BET results, GO leads to an increase in both the hydration degree and MCL. Besides, Raman results confirm the existence of a strong bond between GO and hydration products.

To conclude, considering GO as a nucleation site for the deposition of hydration products at advanced age, resulting in a higher density of C—S—H gel and the establishment of strong bonds between. Furthermore, main chain length (MCL) is also a crucial factor that significantly influences the improvement of mechanical properties. The elongation of main chains confers superior mechanical performance [8,26]. Most research that employed GO as a reinforcing agent provided an explanation for improving the mechanical strength of cement composites through the effect of GO as a nucleation site [7,14,36]. The previous results suggest that the GO-induced modifications of the cement matrix properties at the nanoscale level account for a significant portion of the trends observed at the macro scale experimentally.

Conclusions

The ^{29}Si MAS-NMR tests revealed that the addition of GO increased the main chain length (MCL) value, along as enhanced the hydration degree, at advanced ages, due to its effect as a nucleation site.

The nitrogen adsorption results revealed that the addition of GO increased the BET surface area of the cement paste from 10.42 m^2/g to 12.86 m^2/g. It is obvious, the increase in hydration shows an increase in the specific surface area of C—S—H.

Raman spectroscopy revealed a significant interfacial interaction between GO and (C—S—H) gel of cement paste.

Regarding mechanical strength results, GO was found to be more effective at advanced ages. With the addition of 0.05%,

at 28 and 90 days, an increase in compressive strength by 9.33% and 10.45%, while the flexural strength increased by 19.72% and 21.60% respectively, compared to the reference sample. This enhancement resulted from multiple reinforcing processes for GO, such as increased hydration degree, development of interfacial bonds between GO and hydration products (C–S–H gel), finally, and main chain elongation.

Conflict of interest

The author(s) declare(s) that there is no conflict of interest regarding the publication of this paper.

Acknowledgements

REFERENCES

[1] M.C. Roco, The long view of nanotechnology development: the national nanotechnology initiative at 10 years, in: Nanotechnology Research Directions for Societal Needs in 2020, Springer, Netherlands, 2011, pp. 1–28, http://dx.doi.org/10.1007/978-94-007-1168-6_1.

[2] F. Sanchez, K. Sobolev, Nanotechnology in concrete – a review, Constr. Build. Mater. 24 (2010) 2060–2071, http://dx.doi.org/10.1016/j.conbuildmat.2010.03.014.

[3] T. Meng, K. Ying, X. Yang, Y. Hong, Comparative study on mechanisms for improving mechanical properties and microstructure of cement paste modified by different types of nanomaterials, Nanotechnol. Rev. 10 (2021) 370–384, http://dx.doi.org/10.1515/ntrev-2021-0027.

[4] C. Lin, W. Wei, Y.H. Hu, Catalytic behavior of graphene oxide for cement hydration process, J. Phys. Chem. Solids 89 (2016) 128–133, http://dx.doi.org/10.1016/j.jpcs.2015.11.002.

[5] H.F.W. Taylor, Proposed Structure for Calcium Silicate Hydrate Gel, 1986.

[6] L. Zhao, X. Guo, L. Song, Y. Song, G. Dai, J. Liu, An intensive review on the role of graphene oxide in cement-based materials, Constr. Build. Mater. 241 (2020), http://dx.doi.org/10.1016/j.conbuildmat.2019.117939.

[7] M.M. Mokhtar, S.A. Abo-El-Enein, M.Y. Hassaan, M.S. Morsy, M.H. Khalil, Mechanical performance, pore structure and micro-structural characteristics of graphene oxide nano platelets reinforced cement, Constr. Build. Mater. 138 (2017) 333–339, http://dx.doi.org/10.1016/j.conbuildmat.2017.02.021.

[8] H. Yang, M. Monasterio, D. Zheng, H. Cui, W. Tang, X. Bao, X. Chen, Effects of nano silica on the properties of cement-based materials: a comprehensive review, Constr. Build. Mater. 282 (2021), http://dx.doi.org/10.1016/j.conbuildmat.2021.122715.

[9] G. Land, D. Stephan, The influence of nano-silica on the hydration of ordinary Portland cement, J. Mater. Sci. 47 (2012) 1011–1017, http://dx.doi.org/10.1007/s10853-011-5881-1.

[10] J. Zhou, K. Zheng, Z. Liu, F. He, Chemical effect of nano-alumina on early-age hydration of Portland cement, Cem. Concr. Res. 116 (2019) 159–167, http://dx.doi.org/10.1016/j.cemconres.2018.11.007.

[11] R. Siddique, A. Mehta, Effect of carbon nanotubes on properties of cement mortars, Constr. Build. Mater. 50 (2014) 116–129, http://dx.doi.org/10.1016/j.conbuildmat.2013.09.019.

[12] H. Lee, S. Park, S. Park, W. Chung, Enhanced detection systems of filling rates using carbon nanotube cement grout, Nanomaterials 10 (2020), http://dx.doi.org/10.3390/nano10010010.

[13] Z. Pan, L. He, L. Qiu, A.H. Korayem, G. Li, J.W. Zhu, F. Collins, D. Li, W.H. Duan, M.C. Wang, Mechanical properties and microstructure of a graphene oxide–cement composite, Cem. Concr. Compos. 58 (2015) 140–147, http://dx.doi.org/10.1016/j.cemconcomp.2015.02.001.

[14] W. Li, X. Li, S.J. Chen, Y.M. Liu, W.H. Duan, S.P. Shah, Effects of graphene oxide on early-age hydration and electrical resistivity of Portland cement paste, Constr. Build. Mater. 136 (2017) 506–514, http://dx.doi.org/10.1016/j.conbuildmat.2017.01.066.

[15] S. Stankovich, D.A. Dikin, G.H.B. Dommett, K.M. Kohlhaas, E.J. Zimney, E.A. Stach, R.D. Piner, S.B.T. Nguyen, R.S. Ruoff, Graphene-based composite materials, Nature 442 (2006) 282–286, http://dx.doi.org/10.1038/nature04969.

[16] K. Gong, Z. Pan, A.H. Korayem, L. Qiu, D. Li, F. Collins, C.M. Wang, W.H. Duan, Reinforcing effects of graphene oxide on Portland cement paste, J. Mater. Civil Eng. 27 (2015), http://dx.doi.org/10.1061/(asce)mt.1943-5533.0001125.

[17] X. Kang, X. Zhu, J. Qian, J. Liu, Y. Huang, Effect of graphene oxide (GO) on hydration of tricalcium silicate (C_3S), Constr. Build. Mater. 203 (2019) 514–524, http://dx.doi.org/10.1016/j.conbuildmat.2019.01.117.

[18] H. Yang, M. Monasterio, H. Cui, N. Han, Experimental study of the effects of graphene oxide on microstructure and properties of cement paste composite, Compos. Part A: Appl. Sci. Manuf. 102 (2017) 263–272, http://dx.doi.org/10.1016/j.compositesa.2017.07.022.

[19] Q. Wang, S. Li, J. Wang, S. Pan, C. Lv, X. Cui, Z. Guo, Effect of graphene oxide on hydration process and main hydration products of cement, Kuei Suan Jen Hsueh Pao/J. Chin. Ceram. Soc. 46 (2018) 163–172, http://dx.doi.org/10.14062/j.issn.0454-5648.2018.02.10.

[20] E. Horszczaruk, E. Mijowska, R.J. Kalenczuk, M. Aleksandrzak, S. Mijowska, Nanocomposite of cement/graphene oxide – impact on hydration kinetics and Young's modulus, Constr. Build. Mater. 78 (2015) 234–242, http://dx.doi.org/10.1016/j.conbuildmat.2014.12.009.

[21] UNE-EN 196-1, Métodos de ensayo de cementos. Parte 1: Determinación de resistencias, 2018.

[22] I. KIur, B. Pollet, J. Virlet, A. Nonat, C–S–H structure evolution with calcium content by multinuclear NMR, in: Nuclear Magnetic Resonance Spectroscopy of Cement-based Materials, Springer, Verlag Berlin Heidelberg, 1998, pp. 119–141.

[23] L. Zhao, X. Guo, Y. Liu, Y. Zhao, Z. Chen, Y. Zhang, L. Guo, X. Shu, J. Liu, Hydration kinetics, pore structure, 3D network calcium silicate hydrate, and mechanical behavior of graphene oxide reinforced cement composites, Constr. Build. Mater. 190 (2018) 150–163, http://dx.doi.org/10.1016/j.conbuildmat.2018.09.105.

[24] S. Bae, R. Taylor, D. Kilcoyne, J. Moon, P.J.M. Monteiro, Effects of incorporating high-volume fly ash into tricalcium silicate on the degree of silicate polymerization and aluminum substitution for silicon in calcium silicate hydrate, Materials 10 (2017), http://dx.doi.org/10.3390/ma10020131.

[25] I.G. Richardson, Model structures for C-(A)-S-H(I), Acta Crystallogr. B: Struct. Sci. Cryst. Eng. Mater. 70 (2014) 903–923, http://dx.doi.org/10.1107/S2052520614021982.

[26] I.G. Richardson, Tobermorite/jennite- and tobermorite/calcium hydroxide-based models for the

structure of C–S–H: applicability to hardened pastes of tricalcium silicate, β-dicalcium silicate, Portland cement, and blends of Portland cement with blast-furnace slag, metakaolin, or silica fume, Cem. Concr. Res. 34 (2004) 1733–1777, http://dx.doi.org/10.1016/j.cemconres.2004.05.034.

[27] Z. Yang, Y. Sun, F. Ma, Interlayer spacing of multilayer graphene oxide: influences of oxygen-containing group density, thickness, temperature and strain, Appl. Surf. Sci. 529 (2020), http://dx.doi.org/10.1016/j.apsusc.2020.147075.

[28] B. Lian, S. de Luca, Y. You, S. Alwarappan, M. Yoshimura, V. Sahajwalla, S.C. Smith, G. Leslie, R.K. Joshi, Extraordinary Water Adsorption Characteristics of Graphene Oxide, 2018.

[29] V. Ludwig, J.P.A. de Mendonça, A.H. de Lima, Z.M. da Costa Ludwig, G.M.A. Junqueira, W.G. Quirino, F. Sato, Graphene oxide in water: a systematic computational experimental study, Graphene Technol. 5 (2020) 1–8, http://dx.doi.org/10.1007/s41127-019-00028-7.

[30] X. Li, C. Li, Y. Liu, S.J. Chen, C.M. Wang, J.G. Sanjayan, W.H. Duan, Improvement of mechanical properties by incorporating graphene oxide into cement mortar, Mech. Adv. Mater. Struct. 25 (2018) 1313–1322, http://dx.doi.org/10.1080/15376494.2016.1218226.

[31] X. Zhang, S. Zhou, H. Zhou, D. Li, The effect of the modification of graphene oxide with γ-aminopropyltriethoxysilane (KH550) on the properties and hydration of cement, Constr. Build. Mater. 322 (2022), http://dx.doi.org/10.1016/j.conbuildmat.2022.126497.

[32] Y. Zhao, Y. Liu, T. Shi, Y. Gu, B. Zheng, K. Zhang, J. Xu, Y. Fu, S. Shi, Study of mechanical properties and early-stage deformation properties of graphene-modified cement-based materials, Constr. Build. Mater. 257 (2020), http://dx.doi.org/10.1016/j.conbuildmat.2020.119498.

[33] M.C.G. Juenger, H.M. Jennings, The use of nitrogen adsorption to assess the microstructure of cement paste, Cem. Concr. Res. 31 (6) (2001) 883–892.

[34] R. Kurihara, I. Maruyama, Surface area development of Portland cement paste during hydration: direct comparison with ^{1}H NMR relaxometry and water vapor/nitrogen sorption, Cem. Concr. Res. 157 (2022), http://dx.doi.org/10.1016/j.cemconres.2022.106805.

[35] W. Kurdowski, Cement and Concrete Chemistry, Springer, Netherlands, 2014, http://dx.doi.org/10.1007/978-94-007-7945-7.

[36] X. Li, Y.M. Liu, W.G. Li, C.Y. Li, J.G. Sanjayan, W.H. Duan, Z. Li, Effects of graphene oxide agglomerates on workability, hydration, microstructure and compressive strength of cement paste, Constr. Build. Mater. 145 (2017) 402–410, http://dx.doi.org/10.1016/j.conbuildmat.2017.04.058.

[37] S. Claramunt, A. Varea, D. López-Díaz, M.M. Velázquez, A. Cornet, A. Cirera, The importance of interbands on the interpretation of the Raman spectrum of graphene oxide, J. Phys. Chem. C 119 (2015) 10123–10129, http://dx.doi.org/10.1021/acs.jpcc.5b01590.

[38] G.J. Jing, Z.M. Ye, C. Li, J. Cui, S.X. Wang, X. Cheng, A ball milling strategy to disperse graphene oxide in cement composites, Xinxing Tan Cailiao/New Carbon Mater. 34 (2019) 569–577, http://dx.doi.org/10.1016/S1872-5805(19)60032-6.

[39] K.N. Kudin, B. Ozbas, H.C. Schniepp, R.K. Prud'homme, I.A. Aksay, R. Car, Raman spectra of graphite oxide and functionalized graphene sheets, Nano Lett. 8 (2008) 36–41, http://dx.doi.org/10.1021/nl071822.

[40] Y. Liu, M. Wang, W. Wang, Ohmic heating curing of electrically conductive carbon nanofiber/cement-based composites to avoid frost damage under severely low temperature, Compos. Part A: Appl. Sci. Manuf. 115 (2018) 236–246, http://dx.doi.org/10.1016/j.compositesa.2018.10.008.

[41] F. Banhart, J. Kotakoski, A.V. Krasheninnikov, Structural defects in graphene, ACS Nano 5 (2011) 26–41, http://dx.doi.org/10.1021/nn102598m.